Practical Security Boundary-Constrained DC Optimal Power Flow for Electricity Markets

Miguel Chávez-Lugo, Claudio R. Fuerte-Esquivel, *Senior Member, IEEE*, Claudio A. Cañizares, *Fellow, IEEE*, Victor J. Gutierrez-Martinez

Abstract— **This paper provides a systematic approach to address the fundamental electricity auction issue regarding how to include security boundaries associated with system stability into a security-constrained DC-OPF-based model. These boundaries are linearly approximated by a reduced number of hyperplanes, from which a set of linear inequality security/stability constraints is derived and included into a proposed voltage security-constrained DC-OPF auction model. This allows the proper implementation of a true DC formulation, taking full advantage of its associated simplicity and robustness in the solution algorithm. Case studies are presented to illustrate the applicability of the proposed method and to demonstrate that the market clearing and power dispatch resulting from the optimization solution process are within the desired feasible and secure region, contrary to the typical security constrained DC-OPF auction model, which may fail to meet this condition.**

***Index Terms*— Optimal power flow, power system security, electricity markets, power dispatch.**

I. Introduction

Nowadays, power systems are operating increasingly closer to their control and operational limits because of the increase of power demand and highly competitive electricity markets, which together with other regulatory requirements make new transmission facility construction more difficult. Operating so close to these limits increases the overall operating costs of the power system. Hence, these limits should be properly represented in a security-constrained optimal power flow (SC-OPF) problem [1], since the solution of this problem is used to dispatch generating units in the most economical manner, while satisfying operational and physical constraints of the power system. However, if the security limits are not adequately modeled, the OPF solution may not be secure, i.e. the solution may not guarantee a dispatch that is robust to contingencies.

Several approaches to properly represent the system security in OPF models have been proposed in the literature [2] to obtain optimal security constrained dispatches that assure a secure operation of the power system. In this context, a comprehensive survey of different models and solution techniques used for the SC-OPF problem from early 1960's to 2009 is reported in [3]. The simplest formulations extend the conventional OPF approach by adding a set of steady-state security constraints, such as limits on branch currents and voltage magnitudes, properly modified for each credible contingency considered in the study [4]. This formulation is referred to as the SC-OPF problem [5]. However, the solution of the SC-OPF problem may not yield a secure operating condition [6]-[9], with the voltage stability problem being one of the major security concerns for today's electric power system operation [10]. In order to overcome this drawback, the SC-OPF has been reformulated as a voltage stability-constrained OPF (VSC-OPF) by adding stability constraints derived from voltage stability indices, which quantify how close the current operating point is to voltage instability [7], [11], [12]. In [11], the authors propose the use of a new index to also account for oscillatory stability. These indices, however, represent only one single stress direction corresponding to the dispatch being computed.

In the present restructured power systems, competition between electricity market participants increases the number of possible energy transactions, resulting in different load and generation patterns that may aggravate stability problems caused by high active power transfers or an insufficient reactive power supply. Hence, an alternative approach to achieve a proper representation of system security in this operative context consists of characterizing the entire stability region in the dispatch space, that properly represents multiple load and/or generation patterns [13], [14]. The security/stability boundaries are represented in this case by means of a differentiable function that is included as a constraint in the OPF approach, allowing a secure power system operation, as proposed in [14]. In this formulation, a back-propagation neural network (BPNN) is used to represent the system security/stability boundaries (SB), and an explicit differentiable function is extracted from the BPNN to be used as a security constraint.

In order to avoid the time-consuming process of solving nonlinear OPF models, which may not even yield adequate solutions, a common practice in competitive electricity markets is to adopt DC-OPF formulations, which provide simple and robust solutions to obtain a proper optimal market dispatch [15], [16]. System security in this case is introduced via limits on certain optimization variables, and iterative procedures to account for the system nonlinearities [15]. Thus, a typical SC DC-OPF auction model imposes active power

This work has been supported by Consejo Nacional de Ciencia y Tecnología (CONACyT), México, through the scholarship 218560

Miguel Chávez-Lugo and Claudio R. Fuerte-Esquivel are with the Electrical Engineering Faculty of the Universidad Michoacana de San Nicolás de Hidalgo, Morelia, Mich., México, 58000 (e-mail: miguel@dep.fie.umich.mx, cfuerte@umich.mx).

Claudio. A. Cañizares is with the Department of Electrical and Computer Engineering, University of Waterloo, Waterloo, ON, Canada, N2L3G1 (e-mail: ccanizar@uwaterloo.ca).

Victor J. Gutiérrez-Martínez is with the Department of Electrical Engineering of Instituto Tecnológico de Morelia, Morelia, Mich., México, 58120 (e-mail:vjavier77@yahoo.com.mx).

transfer constraints on transmission lines, which certainly have the most impact on active power dispatch. These limits, however, are determined from off-line studies that do not necessarily correspond to the actual operative system conditions, which may result in inappropriate market signals, jeopardizing system security [15]. Therefore, how to include additional security constraints into the SC DC-OPF auction model is an important issue. In this context, typical single- and multi-period SC DC-OPF auction models were extended in [17] by including the security boundary constraint (SBC) proposed in [14]. Since this constraint is a nonlinear function of the system variables, the resulting SBC auction model is nonlinear, introducing nonlinearities in the SC DC-OPF. Hence, the main motivation of this paper is to obtain a proper and novel linear representation of the security/stability boundaries, which can be readily introduced as a linear constraint in the SC DC-OPF auction and dispatch model.

The adequate linear representation of the aforementioned SB is based on the use of hyperplanes [18], [19], under the assumption that the boundaries are convex [19], resulting in an approximation given by a set of linear inequalities in the multidimensional dispatch space. In order to decrease the dimension of the problem formulation, two new methods to reduce the number of linear constraints to be used in the analytical description of these boundaries are also proposed. Finally, the effectiveness of the proposed approach to obtain an optimal dispatch condition within the secure operating region is demonstrated by means of realistic examples.

The proposed approach is detailed in the rest of this paper, which is structured as follows: Section II briefly describes the typical SC DC-OPF auction linear model, as well as the previously proposed SB formulation. Section III details the procedure for the linear approximation of the security/stability boundaries, along with two proposed approaches to reduce the number of hyperplanes used in this approximation; furthermore, the proposed SBC DC-OPF linear model is also formulated in this section. Study cases are presented in Section IV in order to discuss and compare the results obtained from the application of the proposed techniques. Finally, the main conclusions and contributions of this paper are summarized in Section V.

II. Background

A. Security constrained DC-OPF

The typical single-period SC DC-OPF based auction and dispatch model is formulated as a linear programming problem, consisting of a scalar objective function to be minimized subject to a set of linear equality and inequality constraints, as follows [17]:

$$\min \sum_{i=1}^{n_G} C_{G_i} P_{G_i} \tag{1}$$

s.t.

$$P_{G_k} - P_{L_k} - \sum_{\substack{m=1 \\ m \neq k}}^{n_b} \left(P_{km}^{loss} + b_{km} \left(\delta_k - \delta_m \right) \right) = 0 \quad \forall k \in n_b \tag{2}$$

$$P_{km} - b_{km} \left(\delta_k - \delta_m \right) = 0 \qquad \forall k, m, k \neq m \in n_b \tag{3}$$

$$P_{km}^{\min} \leq P_{km} \leq P_{km}^{\max} \qquad \forall k, m, k \neq m \in n_b \tag{4}$$

$$P_{G_i}^{\min} \leq P_{G_i} \leq P_{G_i}^{\max} \qquad \forall i \in n_G \tag{5}$$

where C_{G_i} is the cost of the *i*-th generator's bid power in \$/MWh; n_b is the number of buses; and n_G is the number of generators, with their individual active power generation represented by P_{G_i} in MW, which cannot exceed its minimum and maximum limits $P_{G_i}^{\min}$ and $P_{G_i}^{\max}$, respectively. Furthermore, P_{G_k} and P_{L_K} are the active power generation and demand at the *k*-th bus, respectively; P_{km} represents the power flowing through the transmission element connecting buses k and m, with its susceptance given by b_{km}; and δ is the bus voltage phasor angle. The system losses cause significant impact on generation dispatch, thus transmission system losses P_{km}^{loss} are incorporated in the auction model by means of a piecewise linear approximation, as detailed in [20], where the system losses are given by:

$$P_{km}^{loss} = g_{km} \sum_{\ell=1}^{L} \alpha_{km}(\ell) \left(\delta_k(\ell) - \delta_m(\ell) \right) \tag{6}$$

with $\alpha_{km}(\ell)$ representing the slope of the ℓ-th segment of the piece wise linear (PWL) approximation, while g_{km} is the conductance of the transmission element connecting buses *k* and *m*. Finally, system security is represented in this model by minimum and maximum power flow limits, $P_{km}^{\min}$ and $P_{km}^{\max}$, respectively, which are calculated off-line by means of loadability and contingency studies.

Participants in the electricity market demand correct market signals for their operational and investment decisions; however, as mentioned before, improper market signals and/or insecure operating conditions may result from this auction model, because its resulting generation dispatch depends on power transfer limits obtained from off-line studies, which do not properly reflect system security for the obtained dispatch. Hence, a proper representation of system security by characterizing security/stability boundaries, from which security constraints are derived considering a variety of generation dispatch patterns, is discussed next.

B. Security Boundary

In the context of electricity markets, as proposed here, another way to properly include security constraints into the DC-OPF formulation is through a linear approximation of the system security boundary. In this case, the boundary is first obtained, and a set of linear constraints are then derived from the linear approximation of the boundary. This set of constraints is then included in the DC-OPF model (1)-(5) in order to assure that the dispatch conditions are within the secure region of operation. The details of how the boundary is obtained are explained next.

Power system security operation requires that the system operates inside a feasibility region F, which is composed of the set of all asymptotically stable equilibrium points that can be reached from a specific initial operating point through the change of system parameters [21]. In this context, this region is defined as a set of load demands and power generations (in the dispatch parameter space) or magnitudes and phase angles of nodal voltages (in the state space), for which the power flow mismatch equations and all types of constraints representing the power system operation are satisfied [22]. This region is bounded by a feasibility boundary Σ, at which the system equilibrium points change their stability properties [21]. Therefore, this feasibility region, and in particular its boundary, is of great importance in the secure operation of the electric power system. A full and detailed description about the computation of the feasibility region and its associated boundary can be found in [13], [14]. Therefore, only the most relevant principles and procedures associated with this computation are discussed here.

The feasibility region and its boundary can be constructed for a specific operating point by identifying equilibrium points, in the parameter space, that are stable with respect to small and large perturbations for a system associated with the following set of differential-algebraic equations representing the power system:

$$\begin{aligned} \dot{\boldsymbol{x}} &= f(\boldsymbol{x}, \boldsymbol{y}, \boldsymbol{\rho}, \boldsymbol{\lambda}) \\ \boldsymbol{0} &= g(\boldsymbol{x}, \boldsymbol{y}, \boldsymbol{\rho}, \boldsymbol{\lambda}) \end{aligned} \tag{7}$$

where $\boldsymbol{x} \in \mathrm{R}^{n_x}$ are the state variables; $\boldsymbol{y} \in \mathrm{R}^{n_y}$ are the algebraic variables; $\boldsymbol{\rho} \in \mathrm{R}^{n_\rho}$ are a set of controllable parameters associated with control device set points; and $\boldsymbol{\lambda} \in \mathrm{R}^{n_\lambda}$ are uncontrollable parameters such as active and reactive power demands. Note that the feasibility region (boundary) corresponds to a stability region (boundary) for stable equilibrium points corresponding to the full base system; for resulting operating points associated with the system with one less element corresponding to the worst contingency (N-1 contingency criteria), the resulting region (boundary) is called the security region (boundary).

The security boundary is computed using a continuation approach, which allows to determine the equilibrium points of (7) that make up the boundary, and thus satisfy the set of equations $0 = f(\cdot)$ and $0 = g(\cdot)$, which include generator and associated control models, as well as the system's AC power flow equations. The stability of these equilibrium points is determined by an eigenvalue analysis of the Jacobian matrix associated with the linearization of (7), and thus the boundary includes a set of equilibrium points associated with codimension-1 generic local bifurcations, i.e. saddle node, Hopf, or limit induced bifurcations, which directly reflect voltage and small-signal angle stability limits. Therefore, each one of these equilibrium points, which defines an operating state of the system, defines a loadability limit representing the system's critical active and reactive powers beyond which the system loses its voltage or angle stability. This boundary is only represented in the P_G-parameter space here due to the fact that generator active powers are the main control variables in the considered OPF model, but voltage and angle stability and the influence of reactive powers are implicitly considered in the security boundary. A detailed explanation of the meaning and calculation of the security boundary can be found in [13].

Despite the fact that end-users may participate in demand response and demand side management programs, or bid on current electricity markets, in practice, load patterns still remain reasonably forecastable in a way that the overall load profile is predictable with reasonable accuracy, so that the market clearing price can be determined by matching a highly elastic supply with a forecast of expected load. In this context, the feasibility region and boundary are then constructed by stressing the system progressively in one particular loading direction at a constant power factor, from the base load scenario, until the instability occurs considering an N-1 contingency criterion and a variety of generation dispatch patterns. Note that the latter permits obtaining a discrete representation of the Σ in the P_G-parameter space.

From the discussion above, the security boundary Σ in the P_G-parameter space can be defined as follows: let $\boldsymbol{\Delta P_{G_k}} = \left[\Delta P_{G_{1,k}} \; \Delta P_{G_{2,k}} \cdots \Delta P_{G_{n_G,k}} \right]^T$ be a k-th particular set of generator power increase rates for all generators participating in the dispatch, where $\Delta P_{G_{i,k}} = \alpha d_{i,k}$ is the power increase rate for the i-th generator from its base generation $P_{G_{i,0}}$, in its corresponding k-th dispatch direction $d_{i,k}$, and $\alpha \geq 0$ is a generation increasing factor. The power output required by the i-th generator to supply a specific load increase from the base load is then given by $P_{G_{i,k}} = \Delta P_{G_{i,k}} P_{G_{i,0}} = \alpha d_{i,k} P_{G_{i,0}}$. In addition, the critical dispatchable generator power output $P^c_{G_{i,k}} = \Delta P^c_{G_{i,k}} P_{G_{i,0}} = \alpha^c d_{i,k} P_{G_{i,0}}$, corresponds to the active power supplied at a loadability limit beyond which the system becomes unstable; hence, $\Delta P^c_{G_{i,k}}$ basically represents the sensitivity of generator i with respect to a loadability limit in the k-th load direction. Note that in order to properly represent multiple generation dispatch patterns, the k-th direction at which the i-th generator is dispatched must lie in the interval $0 \leq d_{ik} \leq 1 \;\; \forall i = 1, \ldots, n_G$, such that $\sum_{i=1}^{n_G} d_{ik} = 1$. Furthermore, a suitable number of different dispatch directions $\boldsymbol{TN}_{dd} = \left[\boldsymbol{d}_1 \, \boldsymbol{d}_2 \cdots \boldsymbol{d}_{n_{dd}} \right]$, where $\boldsymbol{d}_k = \left[d_{1,k} \, d_{2,k} \cdots d_{n_G,k} \right]^T$, must be specified in order to assure that a reasonable density is achieved to get a complete boundary. Based on this, the discrete representation of Σ in the P_G-parameter space is mathematically expressed by the critical active power generation matrix given by (8), where n_{dd} is the number of dispatch directions considered in the study and selected in such a way that a reasonable density to accurately represent Σ is achieved [14]. Note that each column of this matrix defines one boundary point on the discrete Σ in the P_G-parameter space of dimension n_G.

$$M_{CP}=\begin{bmatrix} P^c_{G_{1,1}} & \cdots & P^c_{G_{1,k}} & \cdots & P^c_{G_{1,n_{dd}}} \\ \vdots & \ddots & \vdots & \ddots & \vdots \\ P^c_{G_{i,1}} & \cdots & P^c_{G_{i,k}} & \cdots & P^c_{G_{i,n_{dd}}} \\ \vdots & \ddots & \vdots & \ddots & \vdots \\ P^c_{G_{n_G,1}} & \cdots & P^c_{G_{n_G,k}} & \cdots & P^c_{G_{n_G,n_{dd}}} \\ \uparrow & & \uparrow & & \uparrow \\ \left[\boldsymbol{P}^c_{\boldsymbol{G}_1}\right] & & \left[\boldsymbol{P}^c_{\boldsymbol{G}_k}\right] & & \left[\boldsymbol{P}^c_{\boldsymbol{G}_{n_{dd}}}\right] \end{bmatrix} \quad (8)$$

III. Security Boundary-Constrained DC-OPF Model

A. Linear representation of the security boundary

The linear representation of the feasibility boundary is obtained by its piecewise approximation based on a set of hyperplanes, where each hyperplane in R^{n_G} is completely described by its inclination, which is obtained by specifying a normal vector $\boldsymbol{\eta}$ to the hyperplane, and one boundary point $\boldsymbol{P}^c_{\boldsymbol{G}_k}$ on it [18]. Furthermore, if $\boldsymbol{P}^c_{\boldsymbol{G}_j}$ is an arbitrary boundary point on the hyperplane, $\boldsymbol{P}^c_{\boldsymbol{G}_j}-\boldsymbol{P}^c_{\boldsymbol{G}_k}$ will be a vector in the hyperplane and, consequently, will be perpendicular to $\boldsymbol{\eta}$. Hence, the single linear point-normal equation representing the hyperplane is derived from the dot product given by $\boldsymbol{\eta}\bullet\left(\boldsymbol{P}^c_{\boldsymbol{G}_j}-\boldsymbol{P}^c_{\boldsymbol{G}_k}\right)=\boldsymbol{\eta}\bullet\boldsymbol{P}^c_{\boldsymbol{G}_j}-C=0$, where $C=\boldsymbol{\eta}\bullet\boldsymbol{P}^c_{\boldsymbol{G}_k}$ [18].

In order to obtain the point-normal equation representing each *i*-th hyperplane, finding first its corresponding normal vector $\boldsymbol{\eta}_i$ is necessary. This is achieved by selecting the hyperplane's vertices given by n_G neighboring points of the feasibility boundary Σ, $\boldsymbol{P}^{c,i}_{\boldsymbol{G}_j}\ \forall\ j\in\{n_G$ boundary points$\}$, which are used to find a set of linearly independent (n_G-1) vectors that spans the hyperplane containing them. Based on these vectors, an underdetermined set of (n_G-1) linear equations is formulated and solved for n_G-1 elements of $\boldsymbol{\eta}_i$ and for the constant term C_i, under the assumption that the first element of $\boldsymbol{\eta}_i$ is set to a specified value [18], [19]. A unit value $\eta_{i,1}=1$ has been selected here as proposed in [19].

Considering that the hyperplane's vertices are the n_G boundary points corresponding to the first n_G dispatch directions, $\left[\boldsymbol{P}^{c,i}_{\boldsymbol{G}_1}\ \cdots\boldsymbol{P}^{c,i}_{\boldsymbol{G}_{n_G}}\right]$, and that the boundary point $\boldsymbol{P}^{c,i}_{\boldsymbol{G}_1}$ is the reference hyperplane's vertex from which the (n_G-1) vectors are obtained, as illustrated in Fig. 1 for n_G=3, the set of linearly independent equations to be solved is given, for $j\neq1$, by:

$$\boldsymbol{\eta}_i\bullet\left(\boldsymbol{P}^{c,i}_{\boldsymbol{G}_j}-\boldsymbol{P}^{c,i}_{\boldsymbol{G}_1}\right)=\boldsymbol{\eta}_i\bullet\boldsymbol{P}^c_{\boldsymbol{G}_j}-C_i=0\quad\forall\ j=2,\ldots,n_G \qquad \eta_{i,1}=1 \quad (9)$$

or in matrix form:

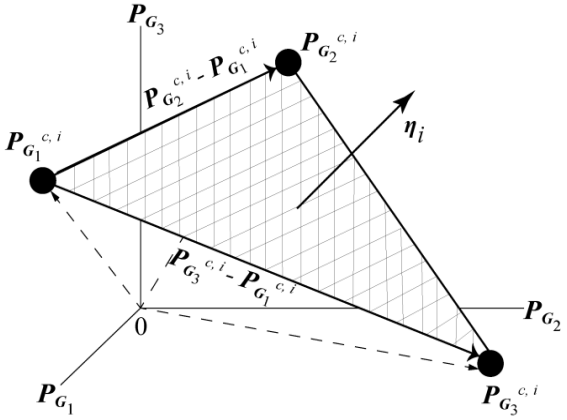


Fig. 1. Hyperplane with vertices $\boldsymbol{P}^{c,i}_{\boldsymbol{G}_1}$, $\boldsymbol{P}^{c,i}_{\boldsymbol{G}_2}$ and $\boldsymbol{P}^{c,i}_{\boldsymbol{G}_3}$.

$$\begin{bmatrix} P^{c,i}_{G_{1,2}} & \cdots & P^{c,i}_{G_{n_G,2}} & -1 \\ \vdots & \ddots & \vdots & \vdots \\ P^{c,i}_{G_{1,n_G}} & \cdots & P^{c,i}_{G_{n_G,n_G}} & -1 \\ 1 & \cdots & 0 & 0 \end{bmatrix}\begin{bmatrix} \eta_{i,1} \\ \vdots \\ \eta_{i,n_G} \\ C_i \end{bmatrix}=\begin{bmatrix} 0 \\ \vdots \\ 0 \\ 1 \end{bmatrix} \quad . \quad (10)$$

Once (10) is solved for n_G-1 elements of $\boldsymbol{\eta}_i$ and the constant term C^i, an *i*-th hyperplane is completely described by:

$$\eta_{i,1}P^{c,i}_{G_{1,n}}+\ldots+\eta_{i,n_G}P^{c,i}_{G_{n_G,n}}=C^i\quad\forall\ i=1,\ldots n_{hy} \quad (11)$$

for any arbitrary boundary point $\boldsymbol{P}^{c,i}_{\boldsymbol{G}_n}$ on the hyperplane, with the set of n_{hy} hyperplanes piecewise-linearly approximating the feasibility boundary Σ.

B. Linear inequalities

Since the operating point resulting from the proposed SBC DC-OPF model must be within the feasibility region F, the active power dispatched by all generators must satisfy the following set of linear inequality constraints, which are directly derived from the set of point-normal equations (11),

$$\eta_{i,1}P_{G_1}+\ldots+\eta_{i,n_G}P_{G_{n_G}}\leq\pm C^i\quad\forall\ i=1,\ldots n_{hy} \quad . \quad (12)$$

The sign on the right side of this inequality constraint will depend of the direction at which the normal vector is pointing to from the feasibility boundary in the P_G-parameter space. If the normal vector points outward (inward) from the feasibility region, the sign is positive (negative). The direction of the normal vector is determined by evaluating (12) considering the generation of active powers that define the base operating point for which the feasibility boundary is computed, $\boldsymbol{P}_{\boldsymbol{G,0}}=\left[P_{G_{1,0}}\quad P_{G_{2,0}}\quad\cdots\quad P_{G_{n_G,0}}\right]^T$. Since $\left\|\boldsymbol{P}_{\boldsymbol{G,0}}\right\|<\left\|\boldsymbol{P}^{c,i}_{\boldsymbol{G}_k}\right\|$, the normal vector $\boldsymbol{\eta}_i$ is pointing outward from the feasibility region if $\boldsymbol{\eta}_i\bullet\boldsymbol{P}^b_{\boldsymbol{G}}<C^i$; otherwise, the direction of $\boldsymbol{\eta}_i$ is inward from the feasibility region.

C. Proposed SBC DC-OPF linear model

The proposed SBC DC-OPF linear dispatch model is formulated based on the set of linear feasibility boundary constraints as follows:

$$\min \sum_{i=1}^{n_G} C_{G_i} P_{G_i} \tag{13}$$

s.t.

$$P_{G_k} - P_{L_k} - \sum_{\substack{m=1 \\ m\neq k}}^{n_b} \left(P_{km}^{loss} + b_{km}\left(\delta_k - \delta_m\right)\right) = 0 \quad \forall k \in n_b \tag{14}$$

$$\sum_{j=1}^{n_G} \eta_{i,j} P_{G_j} \mp C^i \le 0 \qquad \forall i = 1,\ldots n_{hy} \tag{15}$$

$$P_{G_i}^{\min} \le P_{G_i} \le P_{G_i}^{\max} \qquad \forall i \in n_G \tag{16}$$

where (15) represents the voltage feasibility boundary constraints which guarantee that the resulting operating point remains within the feasibility region, as illustrated in Section IV. Note that this constraint replaces (4) in the typical model (1)-(5) to better represent system security. If generators are grouped in generation control areas, (15) is given by:

$$\sum_{k=1}^{n_{G_A}} \left(\eta_{i,k} \sum_{j\in k} P_{Gj}^{A_k} \right) \mp C^i \le 0 \qquad \forall i = 1,\ldots n_{hy} \tag{17}$$

where n_{G_A} is the total number of generation control areas, and $P_{Gj}^{A_k}$ corresponds to the active power produced by the *j*-th generator embedded at the *k*-th generation control area.

The SBC DC-OPF model also incorporates the power loss of each transmission line connecting nodes *k* and *m*, $P_{km}^{loss} \ \forall (k,m) \in n_b$, by means of the piecewise linear approximation proposed in [20]. Hence, for each transmission line, the following set of constraints is included in the set of equations (13)-(17) in order to complete the optimization model:

$$P_{km}^{loss} = g_{km} \sum_{\ell=1}^{L} \alpha_{km}(\ell)\,\delta_{km}(\ell) \tag{18}$$

$$0 \le \delta_{km}(\ell) \le \Delta\delta; \quad \ell = 1,\cdots,L \tag{19}$$

$$\delta_{km} = \left|\delta_k - \delta_m\right| \tag{20}$$

$$\delta_{km} = \sum_{\ell=1}^{L} \delta_{km}(\ell) \tag{21}$$

where L is the number of piecewise linear segments used to represent the power loss in the line, and each ℓ-th segment is defined by its corresponding slope $\alpha_{km}(\ell)$ and its angle increment, given by the difference of phase angles $\delta_{km}(\ell)$. In this case, $\delta_{km}(\ell)$ is a new optimization variable, while $\alpha_{km}(\ell)$ is defined as: $\alpha_{km}(\ell) = (2\ell - 1)\Delta\delta, \quad \ell = 1,\cdots,L$ [20], where $\Delta\delta$ is the maximum angle increment of each segment, i.e. the maximum possible value of $\delta_{km}(\ell)$. Furthermore, δ_{km} is also an optimization variable representing the absolute value of the difference of phase angles at the transmission line's nodes, and this absolute value is also equal to the sum of the value of angle difference in each piecewise linear segment. Finally, constraint (20) is represented by a set of linear constraints, as in [20] and [23], in order to retain the linear properties of the model. Details of the derivation of these equations are given in [20].

D. Dimension of the SBC DC-OPF linear model

The dimension of the optimization problem to be solved is a function of the number of inequality constraints directly associated with the set of hyperplanes used to approximate the feasibility boundary. Hence, reducing the original number of hyperplanes to reduce the dimension of the proposed SBC DC-OPF model is desirable; this is achieved through the following two algorithms.

1) Algorithm 1: Boundary Points' Approximation

1. Each point-normal equation (11) is evaluated at all boundary points composing the discrete SB Σ, i.e. evaluate $\boldsymbol{\eta}_i \bullet \boldsymbol{P}_{\boldsymbol{G}_k}^{c} \ \forall k \in n_{dd}, i \in n_{hy}$.
2. An approximation error criterion is then defined such that $-0.001 \le \boldsymbol{\eta}_i \bullet \boldsymbol{P}_{\boldsymbol{G}_k}^{c} - C^i \le 0$, which defines how far the boundary point from the *i*-th hyperplane is. Note that the maximum limit cannot be bigger than zero; otherwise, the boundary point may be located in the P_G-parameter space below the hyperplane, which implies that an unfeasible region is below the hyperplane, and thus will be considered as a secure region during the optimization process.
3. The hyperplanes are sorted in descending order according to the number of boundary points that satisfy the error criterion.
4. The following criteria are then used to reduce the number of hyperplanes:
   a. The first approximant hyperplane is the one at which the largest number of boundary points satisfies the error criterion. These boundary points are excluded for the subsequent selection of hyperplanes.
   b. For the rest of the boundary points, Step 4a is repeated until all boundary points composing the discrete Σ have been considered.

2) Algorithm 2: Inner Product

1. The inner product of the normal vectors associated with the original set of hyperplanes is calculated.
2. Two normal vectors to their corresponding hyperplanes are considered "parallel" to each other if the angle between them does not exceed five degrees. These normal vectors are then sorted in descending order according to the number of so defined parallel vectors.
3. The following criteria are then used to reduce the number of hyperplanes:
   a. The first approximant hyperplane is the one with the largest number of "parallel" vectors. All hyperplanes associated with this set of normal vectors are excluded for the subsequent selection of hyperplanes.
   b. For the rest of the hyperplanes, Step 3a is repeated until all hyperplanes of the original set have been considered.

Note that the proposed algorithms to linearly approximate the feasibility boundary assure that the boundary points are located on or above the approximant hyperplanes in the P_G-parameter space. From a practical viewpoint, this means that the feasibility region bounded by the hyperplanes $\sum^{hy}$ is always contained within the original feasibility region $\sum$, i.e. $\sum^{hy} \subseteq \sum$.

IV. Results

In order to demonstrate the feasibility and benefits of the proposed SBC DC-OPF model, the IEEE 3-machine 9-bus test system [24], and the IEEE 54-machine 118-bus test system [25] are used here as examples. Additionally, the typical SC DC-OPF reported in Section II and the Neural Network-Based Security Boundary Constrained DC-OPF model presented in [17] are used to compare and to validate the proposed model and its results.

A. IEEE 3-machine 9-bus test system

This system is composed of three generators at Buses 1, 2, and 3, with active power output limits of 900 MW, 700 MW and 600 MW, respectively, and three loads at buses 5, 6, and 8, as shown in Fig. 2. The system is divided into three generation areas directly related to each generator, i.e. areas A, B, and C corresponding to generators G_1, G_2, and G_3, respectively. All data for this system are reported in [24]. The system stability boundary was obtained following the procedure discussed in Section II.B, based on static and dynamic studies (an exciter model Type II was used), assuming that the loading increments are supplied from 631 different generation dispatches at each generation area.

The stability boundary for this system is shown in Fig. 3, while the total number of hyperplanes required to approximate this boundary by brute force, boundary points' approximation, and inner product approaches, respectively, is illustrated in Table I. Note that a reduction of 79% and 91% in the number of approximant hyperplanes is achieved by the boundary points' approximation and inner product approaches with respect to the brute force approach, respectively. The absolute errors between the boundary points composing Σ and their corresponding approximant hyperplanes is obtained by:

$$\frac{\left|\boldsymbol{\eta}_i \bullet \boldsymbol{P}_{\boldsymbol{G}}^{\boldsymbol{c},\boldsymbol{i}} - C^i\right|}{C^i} \quad \forall i = 1,\ldots n_{hy} \qquad (22)$$

and these are reported in Figs. 4 and 5 for the boundary points' approximation and inner product approaches, respectively. Note that the maximum absolute error of the boundary points' approximation does not exceed 0.25%, proving that the approximation is fairly accurate. Moreover, the maximum absolute error related to the application of the inner product approach is below 0.9%; this increment with respect to the boundary points' approximation is due to the minimum number of hyperplanes employed to perform the linear approximation of Σ, so that each hyperplane approximates a greater number of boundary points.

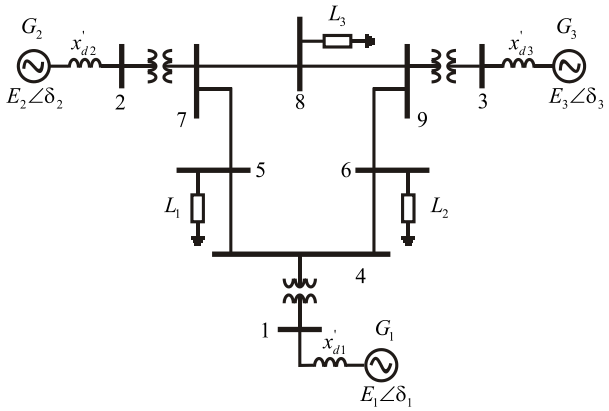


Fig.2. On-line diagram of the IEEE 3-machine 9-bus test system.

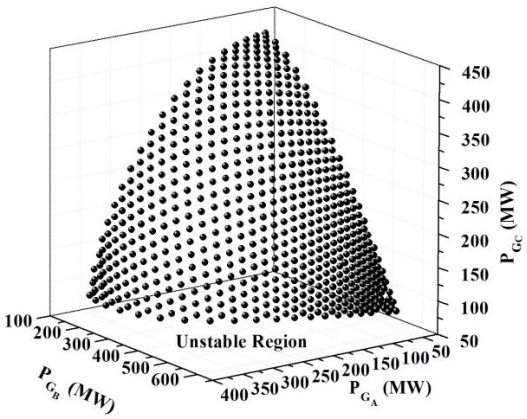


Fig.3. Stability boundary for the IEEE 9-bus system.

TABLE I
NUMBER OF $\sum^{hy}$ FOR THE IEEE 9-BUS SYSTEM $\sum$

Approximation Approach	Number of planes
Brute Force	630
Boundary Points' Approximation	132
Inner Product	52

TABLE II
LINEAR SBC DC-OPF DISPATCH RESULTS FOR THE IEEE 9-BUS SYSTEM

Approximation Approach	P_{G_A} (MW)	P_{G_B} (MW)	P_{G_C} (MW)	Losses (MW)	Generation Cost ($/h)
Brute Force	322.638	182.319	188.221	13.578	988.680
Boundary Points' Approximation	323.081	181.254	188.837	13.572	988.567
Inner Product	333.381	163.000	196.750	13.531	986.683

For a base load increment of 60%, the proposed optimization model is solved considering, independently, each set of linear inequality constraints related to each of the three piecewise-linear approximation approaches. The generation dispatches of each area, system losses and optimal generation cost obtained are reported in Table II. Note that the most economical generation dispatch corresponds to the inner product approach, presenting the lowest transmission losses and lowest cost of the most expensive generator with respect to the results obtained with the brute force and boundary points' approximation approaches.

The system under study was analyzed using the SC DC-OPF linear model reported in Section II and the SBC DC-OPF nonlinear model detailed in [17]. Both models validate the results obtained by the proposed approach for the

brute force approach. The results for each model are shown in Table III, in terms of the generation dispatch, system losses, and total generation costs, and the "location" of these generation dispatches in the P_G-parameter space is shown in Fig. 6. Note that the typical SC DC-OPF linear model provides the most economical dispatch, but it is infeasible as it is outside the stability region, as shown in Fig. 6. On the other hand, the solutions obtained with the nonlinear and linear SBC DC-OPFs are feasible in terms of system stability, with the nonlinear approach to model the stability boundary being the one that provides the most economic operating point.

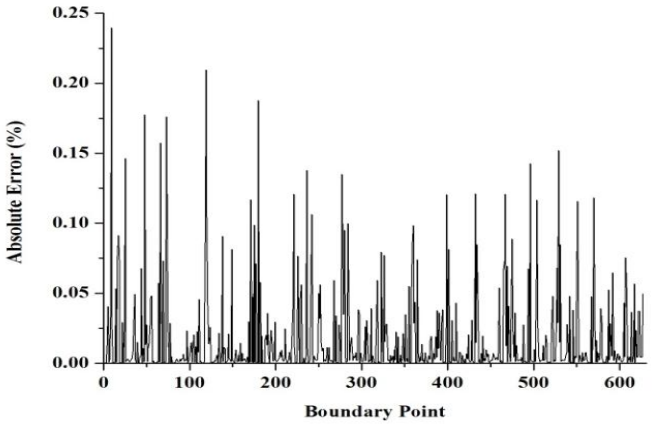


Fig. 4. Absolute error with the boundary points' approximation.

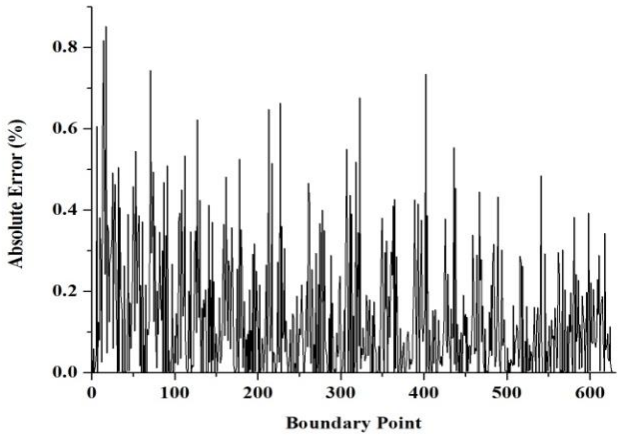


Fig. 5. Absolute error with the inner product approach.

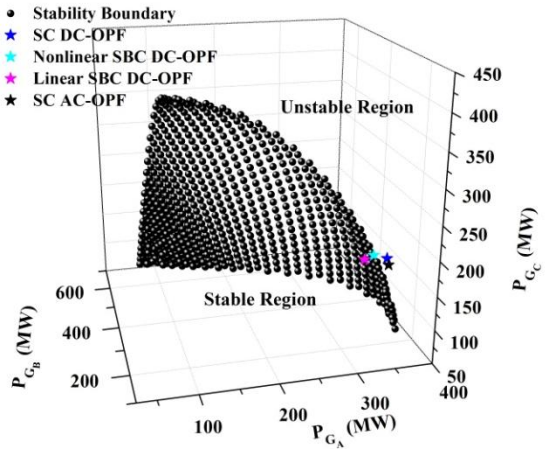


Fig.6. Dispatch solutions and their location in the P_G-parameter space for the IEEE 9-bus system.

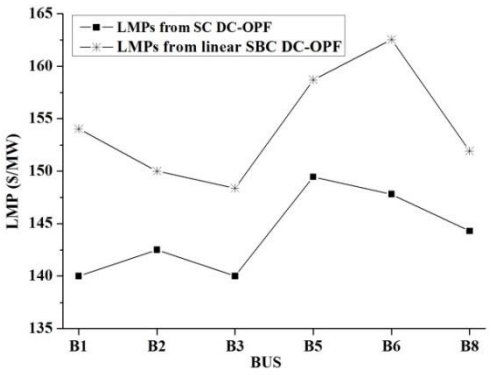


Fig. 7. LMPs for the IEEE 9-bus system for both the SC DC-OPF and the proposed linear SBC DC-OPF.

Figure 7 compares the Locational Marginal Prices (LMPs) at all generator and load buses for both the SC DC-OPF and the proposed linear SBC DC-OPF. The values of these LMPs correspond to the Lagrange multipliers associated with the active power balance constraints at the generator and load buses. Observe that both yield, for all practical purpose, very similar results, with the proposed approach generating slightly higher LMPs. This is to be expected, since it can be observed in Fig. 6 that the solutions are close, with the proposed technique being the most constrained by the stability boundary. Similar results were obtained for the other cases discussed next.

These results highlight the impact of properly considering system stability (or security) constraints in the optimization model, demonstrating that a feasible solution not only depends on the active power demanded by the system and its corresponding generation dispatch, but also on the system stability (or security) constraints. Tables IV and V provide the CPU times required by the DC-OPF models and the proposed SBC DC-OPF approaches, respectively. All OPF models were solved using AMPL [26] with the KNITRO solver [27] in a computer with a 2.93GHz CPU and 16 GB of RAM.

TABLE III
DC-OPF SOLUTIONS FOR THE IEEE 9-BUS SYSTEM

OPF Model	P_{G_A} (MW)	P_{G_B} (MW)	P_{G_C} (MW)	Losses (MW)	Generation Cost ($/h)
SC DC-OPF	340.930	163.000	189.096	13.426	986.536
Nonlinear SBC DC-OPF	330.113	164.423	198.628	13.564	986.872
Linear SBC DC-OPF	322.638	182.319	188.221	13.578	988.680

TABLE IV
CPU TIMES FOR THE VARIOUS DC-OPF MODELS FOR THE IEEE 9-BUS SYSTEM

OPF Model	Time (ms)
SC DC-OPF	8.86
Nonlinear SBC DC-OPF	7.95
Linear SBC DC-OPF	32.08

TABLE V
CPU TIMES FOR THE LINEAR SBC DC-OPF APPROACHES FOR THE IEEE 9-BUS SYSTEM

Approximation Approach	Time (ms)
Brute Force	32.08
Boundary Points' Approximation	15.98
Inner Product	13.69

TABLE VI
LINEAR SBC DC-OPF DISPATCH FOR THE IEEE 9-BUS SYSTEM WITH CONTINGENCY

Approximation Approach	P_{G_A} (MW)	P_{G_B} (MW)	P_{G_C} (MW)	Losses (MW)	Generation Cost ($/h)
Brute Force	227.532	224.329	97.119	9.547	791.005
Boundary Points' Approximation	226.796	194.329	127.442	9.134	787.427
Inner Product	230.654	196.508	121.364	9.094	787.587

TABLE VII
DC-OPF SOLUTIONS FOR THE IEEE 9-BUS SYSTEM WITH CONTINGENCY

OPF Model	P_{G_A} (MW)	P_{G_B} (MW)	P_{G_C} (MW)	Losses (MW)	Generation Cost ($/h)
SC DC-OPF	277.829	163.000	107.055	8.452	783.338
Nonlinear SBC DC-OPF	227.089	196.883	124.610	9.149	787.702
Linear SBC DC-OPF	227.532	224.329	97.119	9.547	791.005

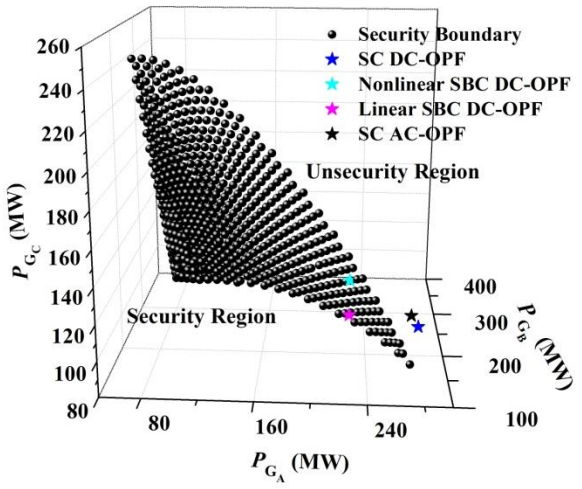


Fig.8. Security boundary and dispatch solutions for the IEEE 9-bus system.

The study was repeated considering a contingency corresponding to the tripping of the line connecting nodes 5-7. Hence, the system's stability boundary in Fig. 6 becomes the security boundary shown in Fig. 8, which required 630, 80, and 20 hyperplanes to approximate it using the brute force, boundary points' approximation, and inner product approaches, respectively. In this case, the maximum absolute errors between the security boundary points and their corresponding approximant hyperplanes were 0.23247% and 0.7304% for the boundary points' approximation and inner product approaches, respectively. Table VI shows the optimal generation dispatch obtained with the proposed linear SBC DC-OPF while considering the security constraints associated with each linear representation of the security boundary for a base load increment of 27%; the most economical dispatches correspond to the cases where the security constraints are derived from the linear approximations associated with the use of approximant hyperplanes. The numerical comparisons of the results obtained with the proposed linear SBC DC-OPF using the brute force approximation with the results obtained with the SC DC-OPF and the SBC DC-OPF nonlinear model are reported in Table VII; observe in Fig. 8 that the SC DC-OPF yields an unsecure dispatch, i.e. the corresponding solution is located outside the security region.

TABLE VIII
SC AC-OPF SOLUTIONS FOR THE IEEE 9-BUS SYSTEM

Study Case	P_{G_A} (MW)	P_{G_B} (MW)	P_{G_C} (MW)	Losses (MW)	Generation Cost ($/h)
Base system	350.170	163.000	182.857	16.427	990.738
System with contingency	272.261	163.000	113.366	9.195	784.379

Lastly, the study cases detailed above have been analyzed using an SC AC-OPF approach. Thus, Table VIII shows the optimal generation dispatches when the base system as well as the system with the reported single contingency scenario are considered, respectively; the location of the corresponding system's operating points in the P_G-parameter space is shown in Figs. 6 and 8. Observe that these solutions are similar to the SC DC-OPF solutions and lie outside the security region in the system P_G-parameter space. These results demonstrate that, as with the SC DC-OPF, the SC AC-OPF is unable to properly account for the actual system security limits.

B. IEEE 54-machine 118-bus test system

The IEEE 54-machine 118-bus test system from [25] is used here to prove the effectiveness of the proposed approach when dealing with a more realistic and larger power system. This system was divided into three operational areas with 18 generators each. A static voltage security boundary was obtained for the worst single contingency, corresponding to a Line 39-40 trip. A total of 631 different generation directions for each area were considered in the computation of Σ. The resulting security boundary is depicted in Fig. 9, while the number of hyperplanes required for its linear approximation is shown in Table IX. Note that the boundary points' approximation and inner product approaches reduce the number of hyperplanes by 76% and 96%, with respect to the brute force methodology, respectively. As expected, the boundary points' approximation is the one with the smallest errors, which do not exceed 2.4%, as shown in Fig. 10, whereas the errors do not exceed 9.8% when the inner product approach is applied, as shown in Fig. 11; the errors for the latter approach are due to the larger reduction in the total number of hyperplanes used to represent Σ.

The dispatch solutions regarding the three approximation approaches, considering a 15% increment in the system's base load, are shown in Table X. In this case, all generators have been assumed to have different production costs in the range of 0.3 to 0.8 $/MWh. For comparison purposes, an SC AC-OPF and the SC DC-OPF and linear SBC DC-OPF models were used to obtain the optimal generation dispatches for this loading scenario, with the corresponding solutions being shown in Table XI; the "location" of the corresponding dispatches in the P_G-parameter space are depicted in Fig. 9. Note that the SC AC-OPF model provides the most economic operating point, but also the most insecure generation dispatch. On the other hand, the SC DC-OPF model provides the most expensive solution, which is also located outside the security region of operation but closer to the security boundary. Lastly, and in contrast to the insecure solutions obtained with the SC AC-OPF and SC DC-OPF models, the solution obtained with the linear SBC DC-

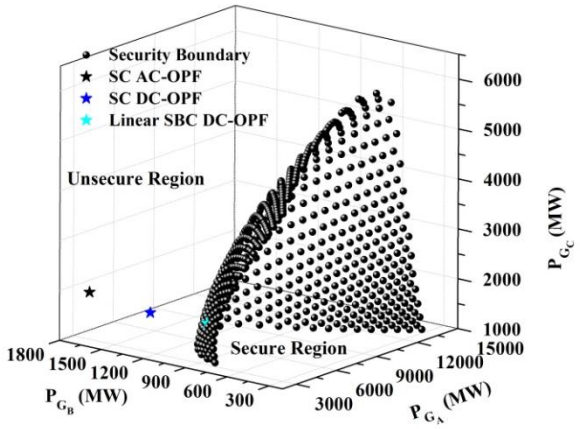


Fig. 9. Security boundary and dispatch solutions for the IEEE 118-bus system.

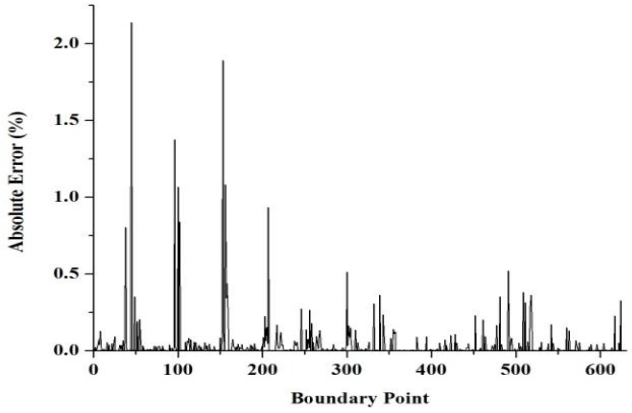


Fig. 10. Absolute error with the boundary points' approximation for the IEEE 118-bus system.

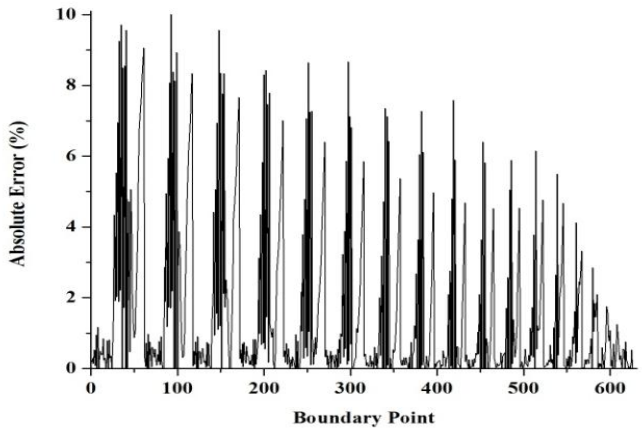


Fig. 11. Absolute error with the inner product approach for the IEEE 118-bus system.

OPF model lies in the feasible region of operation. These results clearly show the suitability of the proposed optimization model to obtain a secure operating point for a given set of loading conditions.

Even though one would intuitively expect to sacrifice economic gain for security, the reason for the non-intuitive behavior in the results associated with the DC-based OPF models and summarized in Table XI and Fig. 9 is that the proposed approach reduces the amount of generation in Areas B and C in order to maintain the operation within the secure operating region, resulting on the generation costs for each area reported in Table XII, where it is possible to infer that the generation cost in Areas B and C is reduced by 114.31 $/h and 12.7 $/h, respectively. However, to supply the required demand, generation in Area A is increased, resulting in a cost increment of 123.9 $/h. Since the reduction in the generation cost of areas B and C is higher than the increment in area A, the system security is preserved while reducing overall operating costs. This is not observed when the SC DC-OPF is employed to obtain the optimal dispatch.

The CPU times required by the SC DC-OPF and linear SBC DC-OPF models are reported in Tables XIII and XIV, respectively, for the aforementioned computer system.

TABLE IX
NUMBER OF $\sum^{hy}$ FOR THE IEEE 118-BUS SYSTEM $\sum$

Approximation Approach	Number of planes
Brute Force	630
Boundary Points' Approximation	153
Inner Product	25

TABLE X
DISPATCH RESULTS FOR THE IEEE 118-BUS SYSTEM

Approximation Approach	P_{G_A} (MW)	P_{G_B} (MW)	P_{G_C} (MW)	Losses (MW)	Generation Cost ($/h)
Brute Force	3096.140	848.939	1816.800	139.025	1775.755
Boundary Points' Approximation	3156.700	861.471	1766.500	161.815	1783.309
Inner Product	3141.140	859.914	1765.340	143.535	1777.921

TABLE XI
OPF SOLUTIONS FOR THE IEEE 118-BUS SYSTEM

OPF Model	P_{G_A} (MW)	P_{G_B} (MW)	P_{G_C} (MW)	Losses (MW)	Generation Cost ($/h)
SC AC-OPF	2030.450	1587.030	2089.120	83.740	1713.280
SC DC-OPF	2694.120	1217.990	1844.460	133.714	1778.863
Linear SBC DC-OPF	3096.140	848.939	1816.800	139.025	1775.755

TABLE XII
GENERATION COSTS FOR THE IEEE 118-BUS SYSTEM.

OPF Model	Generation costs			
	Area A ($/h)	Area B ($/h)	Area C ($/h)	Total Cost ($/h)
SC AC-OPF	601.93	518.61	592.74	1713.28
SC DC-OPF	809.57	411.54	557.74	1778.86
Linear SBC DC-OPF	933.47	297.23	545.03	1775.74

TABLE XIII
CPU TIMES FOR THE VARIOUS DC-OPF MODELS FOR THE 118-BUS SYSTEM

OPF Model	Time (s)
SC DC-OPF	0.33139
Linear SBC DC-OPF	1.85205

TABLE XIV
CPU TIMES FOR THE LINEAR SBC DC-OPF APPROACHES FOR THE 118-BUS SYSTEM

Approximation Approach	Time (s)
Brute force	1.85205
Boundary points' approximation	1.25721
Inner product	0.65581

TABLE XV
OPF SOLUTIONS FOR THE IEEE 54-MACHINE 118-BUS SYSTEM WITH DIFFERENT GENERATION COSTS

OPF Model	P_{G_A} (MW)	P_{G_B} (MW)	P_{G_C} (MW)	Losses (MW)	Generation Cost ($/h)
SC AC-OPF	1881.0	2685.29	1282.64	226.07	1217.62
SC DC-OPF	2397.77	1472.85	1880.04	127.81	1430.63
Linear SBC DC-OPF	3383.02	919.52	1476.80	156.48	1549.90

TABLE XVI
GENERATION COSTS FOR THE IEEE 54-MACHINE 118-BUS SYSTEM WITH DIFFERENT GENERATION COSTS

OPF Model	Generation costs			
	Area A ($/h)	Area B ($/h)	Area C ($/h)	Total Cost ($/h)
SC AC-OPF	564.30	268.53	384.79	1217.62
SC DC-OPF	719.33	147.28	564.01	1430.63
Linear SBC DC-OPF	1014.91	91.95	443.04	1549.90

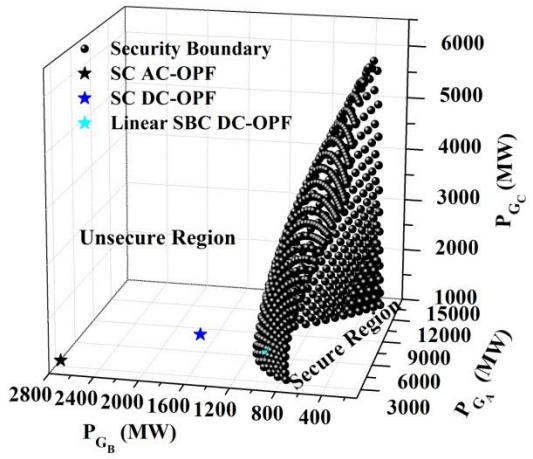


Fig. 12. Security boundary and dispatch solutions for the IEEE 54-machine 118-bus system with different generation costs.

Independently of the cost of generation in Area B, the proposed approach will tend to reduce the generation of active power in this area to maintain system security. In order to validate this statement, the previous study has been repeated considering a production cost of 0.1 $/MWh for all generators in Area B and of 0.3 $/MWh for all generators located in Areas A and C; the results are reported in Tables XV and XVI. The location of the power generation dispatches in the P_G-parameter space is shown in Fig. 12. Observe that this results in the proposed approach sacrificing economic gain due to system security, as intuitively expected, resulting in an optimal operating point that is more expensive than the one obtained with the SC DC-OPF. The latter, however, yields an optimal operating point outside the security region.

Note that the proposed approach provides an optimal economic generation dispatch that is secure, in all cases, as opposed to the "standard" SC DC- and AC-OPFs, which yield insecure dispatches. This unique attribute of the proposed method is possible because of the proper characterization and linearization of the security/stability region for multiple load and/or generation patterns, which is included in the OPF as an additional constraint. An economic consequence of systems working close to their stability/security boundaries, as depicted in Figs. 9 and 12 for the 118-bus system, is that these systems are more constrained (congested) and hence more expensive to operate. In fact, the SC DC- and AC-OPF solutions will require adjustments by the operator to make them secure, thus increasing operating costs.

V. CONCLUSIONS

This paper proposed a DC OPF-based approach that properly considers system security/stability boundaries. These nonlinear boundaries have been represented by a set of point-normal equations of hyperplanes to linearized the boundaries and include them as linear inequality security/stability constraints into a proposed SBC DC-OPF model. Practical methodologies and procedures have also been proposed to reduce the number of hyperplanes required to linearly approximate the power system security/stability boundaries, which substantially reduce the dimension of the proposed linear optimization model.

The discussed numerical examples illustrate the effectiveness of the proposed piecewise linear SBC DC-OPF auction model demonstrating its merits with respect to a DC OPF-based auction models used in practice. The presented case studies and their results show that the proposed auction algorithm ensures that the resulting operating points are optimal from both the economical and security points of view. Therefore, this auction model should provide system operators with a more complete and reliable support tool for market clearing and power dispatch.

An essential feature of smart grids is to enable demand response and demand side management, with loads varying following both prices and end-user preferences, and hence these can no longer be considered constant. Therefore, proper load models for OPF applications such as the one described here are needed to adequately reflect the interaction between markets and end users; the authors are currently pursuing this work in the same context as the current paper, i.e. the development of improved and practical OPF models.

VI. REFERENCES

[1] J. L. Martínez-Ramos and V. H. Quintana, "Optimal and secure operation of transmission systems," in: A. Gómez-Expósito, A. Conejo and C. Cañizares, Eds., *Electric Energy Systems: Analysis and Operation.* Boca Raton, FL:CRC, 2009, pp. 211-264.

[2] B. Stott, O. Alsac, and A. Monticelli, "Security analysis and optimization," *Proc. of the IEEE*, Vol. 75, no. 12, pp. 1623-1644, Dec. 1987.

[3] M.M. Bhaskar, M. Srinivas, and S. Maheswarapu, "Security constrained optimal power flow (SCOPF)-A comprehensive survey," *Int. J. Comp. App.,* vol. 11, no. 3, pp. 42-62, Dec. 2010.

[4] O. Alsac and B. Stott, "Optimal load flow with steady-state security," *IEEE Trans. Power App. Syst*., vol. PAS-93, no. 3. Pp. 745-751, May 1974.

[5] A. J. Monticelli, M. V. P. Pereira, and S. Granville, "Security-constrained optimal power flow with post-contingency corrective rescheduling," *IEEE Trans. Power Syst.*, vol. 2, no. 1, pp. 175-182, Feb. 1987.

[6] D. Gan, R. J. Thomas, and R. D. Zimmerman, "Stability-constrained optimal power flow," *IEEE Trans. Power Syst.*, vol.15, no.2, pp.535-540, May 2000.

[7] W. Rosehart, C. Cañizares, and V. Quintana, "Optimal power flow incorporating voltage collapse constraints," in *Proc. 1999 IEEE PES Summer Meeting*, pp. 820-825.

[8] F. Milano, C. A. Cañizares, and A. J. Conejo, "Sensitivity-based security-constrained OPF market clearing model," *IEEE Trans. Power Syst.*, vol.20, no.4, pp.2051-2060, Nov. 2005.

[9] D. Chattopadhyay and G. Deqiang, "Dispatch optimization incorporating transient and voltage stability constraints," in *Proc. 2000 IEEE PES Summer Meeting*, pp. 516-521.
[10] Y. Besanger, M. Eremia, and N. Voropai, "Major grid blackouts: Analysis, classification, and prevention," in: M. Eremia and M. Shahidehpour, Eds., *Handbook of Electrical Power System Dynamics: Modeling, Stability, and Control.* Hoboken, NJ:Wiley-IEEE press, 2013, pp.789-863.
[11] C. Cañizares, W. Rosehart, A. Berizzi, and C. Bovo, "Comparison of voltage security constrained optimal power flow techniques," in *Proc. 2001 IEEE PES, Summer Meeting*, pp. 2115-2120.
[12] R. J. Avalos, C. A. Cañizares, and M. F. Anjos, "A practical voltage-stability-constrained optimal power flow," in *Proc. 2008 IEEE PES, General Meeting*, pp. 1-6.
[13] X. Gu, and C. A. Cañizares, "Fast Prediction of Loadability Margins Using Neural Networks to Approximate Security Boundaries of Power Systems," *IET Gen., Trans. Dist.*, vol. 1, no. 3, pp. 466-475, May 2007.
[14] V. J. Gutierrez-Martinez, C. A. Cañizares, C. R. Fuerte-Esquivel, A. Pizano-Martínez, and X. Gu, "Neural-network security-boundary constrained optimal power flow," *IEEE Trans. Power Syst.*, vol.26, no.1, pp. 1944-1954, Feb. 2011.
[15] C. A. Cañizares and S. K. M. Kodsi, "Power system security in market clearing and dispatch mechanisms," in *Proc. 2006 IEEE PES Power Syst. Conf. Expo.*, pp. 1-6.
[16] B. Stott and O. Alsac, "Optimal Power Flow—Basic Requirements for Real-life Problems and their Solutions," white paper, July 2012. [On Line.] Available: www.ieee.hr/_download/repository/Stott-Alsac-OPF-White-Paper.pdf
[17] C. Battistelli, C. A. Cañizares, M. Chehreghani-Bozchalui, V. J. Gutierrez-Martinez, and C. R. Fuerte-Esquivel, "Practical Security-Boundary-Constrained Dispatch Models for Electricity Markets," in *Proc. Power Syst. Comp. Conf.*, 2011, pp. 1-7.
[18] C. P. Simon and L. Blume, *Mathematics for economists.* New York, NY: W. W. Norton& Company, Inc., 1994, pp. 226-230.
[19] Y. Makarov, P. Du, S. Lu, T. B. Nguyen, X. Guo, J. W. Burns, and J. F. Gronquist. "Wide area security region," Pacific Northwest National Lab., USA, March 2010. [Online.] Available: http://www.pnl.gov/main/publications/external/technical_reports/PNNL-19331.pdf
[20] A. Motto, F. Galiana, A. Conejo, and J. Arroyo, "Network-constrained Multiperiod Auction for a Pool-Based Electricity Market," *IEEE Trans. Power Syst.*, vol.17, no. 3, pp. 646-653, Aug. 2002.
[21] V. Venkatasubramanian, H. Schättler, and J. Zaborsky, "Local Bifurcations and Feasibility Regions in Differential-Algebraic Systems," *IEEE Trans. on Automatic Cont.*, vol. 40, no. 4, pp. 1992-2013, Dec. 1995.
[22] F. Wu and S. Kumagai, "Steady-state security regions of power systems," *IEEE Trans. Circuits Syst., I: Fund. Theory Appl.*, vol.29, no.11, pp. 703-711, Nov. 1982.
[23] D. Bertsimas and J.N. Tsitsiklis, *Introduction to Linear Optimization.* Belmont MA: Athena Scientific, 1997, pp. 17-19.
[24] P. W. Sauer and M. A. Pai, *Power System Dynamics and Stability*. Upper Saddle River, NJ: Prentice-Hall, 1998, pp.171-177.
[25] [Online.] Available: http://www.ee.washington.edu/research/pstca/.
[26] R. Fourer, D. M. Gay, and B. W. Kernighan, *AMPL: A Modeling Language for Mathematical Programming*, 2nd ed. Pacific Grove, CA: Thomson, Brooks/Cole, 2003.
[27] KNITRO. [Online.] Available: http://www.ziena.com

BIOGRAPHIES

Miguel Chávez-Lugo received the B.Eng. degree from the Instituto Tecnológico de Morelia, Morelia, México, in 2008, the MS degree from the Universidad Michoacana de San Nicolás de Hidalgo (UMSNH), Morelia, México, in 2010. He is currently pursuing the Ph.D. degree at the Universidad Michoacana de San Nicolás de Hidalgo in the areas of voltage stability and electricity markets in power systems.

Claudio R. Fuerte-Esquivel (M'1991-SM'04) received his BEng degree (Hons) from Instituto Tecnológico de Morelia, México in 1990, his M.Sc. degree (Summa Cum Laude) from Instituto Politécnico Nacional, México in 1993, and his Ph.D. degree from the University of Glasgow, Scotland, UK in 1997. Currently, he is a full-time professor at Universidad Michoacana, where his research interests lie on the dynamic and steady-state analysis of FACTS.

Claudio A. Cañizares (S'86-M'91-SM'00-F'07) received the Electrical Engineer degree from Escuela Politécnica Nacional (EPN), Quito-Ecuador, in 1984 where he held different teaching and administrative positions from 1983 to 1993. His MSc (1988) and PhD (1991) degrees in Electrical Engineering are from University of Wisconsin-Madison. He has been with the E&CE Department, University of Waterloo since 1993, where he has held various academic and administrative positions and is currently a full Professor and the Associate Director of the Waterloo Institute for Sustainable Energy (WISE). He was awarded Hydro One research chair in 2010. His research activities concentrate in the study of stability, modeling, simulation, control and computational issues in power systems within the context of competitive electricity markets and smart grids. He is a Fellow of the Royal Society of Canada and the Canadian Academy of Engineering.

Victor J. Gutierrez-Martinez received the B.Eng. (Hons.), M.S., and Ph.D degrees from the Universidad Michoacana de San Nicolás de Hidalgo (UMSNH), Morelia, México, in 2000, 2004, and 2011, respectively. From June 2007 to May 2008, he was a visiting student at the University of Waterloo, Waterloo, ON, Canada, and a Postdoctoral Fellow from 2012 to 2013 working on smart grid topics. He joined to the Department of Electrical Engineering of the Technological Institute of Morelia, Morelia, Mich., Mexico, in 2013, where he is currently a full time Professor. His research interests are in power system modeling and operational aspects in the context of smart grids.